

THE INFLUENCE OF GAS DYNAMICS ON MEASURING THE PROPERTIES OF THE BLACK HOLE IN THE CENTER OF THE MILKY WAY WITH STELLAR ORBITS AND PULSARS

DIMITRIOS PSALTIS

Astronomy Department, University of Arizona, 933 N. Cherry Ave., Tucson, AZ 85721, USA

Draft version December 2, 2011

ABSTRACT

Observations of stars and pulsars orbiting the black hole in the center of the Milky Way offer the potential of measuring not only the mass of the black hole but also its spin and quadrupole moment, thereby providing observational verification of the no-hair theorem. The relativistic effects that will allow us to measure these higher moments of the gravitational field, however, are very small and may be masked by drag forces that stars and pulsars experience orbiting within the hot, tenuous plasma that surrounds the black hole. The properties of this plasma at large distances from the central object have been measured using observations of the extended X-ray emission that surrounds the point source. At distances comparable to the black-hole event horizon, the properties of the accretion flow have been constrained using observations of its long-wavelength emission and polarization, as well as of the size of the emitting region at 1.3 mm. I use models of the plasma density and temperature at various distances from the black hole to investigate the effect of hydrodynamic drag forces on future measurements of the higher moments of its gravitational field. I find that hydrodynamic drag does not preclude measurements of the black hole spin and quadrupole moment using high-resolution observations of stars and pulsars that orbit within a few thousand gravitational radii from its horizon.

Subject headings: TBD

1. INTRODUCTION

The black hole in the center of the Milky Way, Sgr A* has a number of characteristics that make it an ideal candidate for testing general relativity in the strong field regime. It is surrounded by a swarm of young stars at very close orbits, the tracking of which has already led to a direct measurement of its mass (see Ghez et al. 2008; Gillessen et al. 2009 for recent work). It is accreting from the surrounding medium at rates high enough to make it a detectable source both in the X-rays (e.g., Baganoff et al. 2003) and at long wavelengths (e.g., Falcke et al. 2008; Yusef-Zadeh et al. 2009). It is also the black hole with a horizon that subtends the largest angle in the sky, making it possible to directly image the region very close to its horizon (e.g., Doeleman et al. 2008).

Three distinct technological advances in the next decade offer the possibility of not only improving the accuracy of our knowledge of the black hole's mass but also of measuring directly its spin and quadrupole moment. This last quantity of the gravitational field is not an independent quantity in the Kerr metric; instead it depends in a very particular way on the mass and spin of the black hole, as required by the no-hair theorem (see, e.g., Ryan 1995). Measuring all three moments of the spacetime of Sgr A* will, therefore, allow us to test the black-hole nature of the source, verify the validity of the no-hair theorem, and consequently test general relativity in the strong-field regime (see Will 1998; Psaltis & Johannsen 2011).

Interferometric observations in large telescopes equipped with adaptive optics (such as GRAVITY on the VLT; Gillessen et al. 2010) will detect and track stars in very close orbits around Sgr A*. The orbits of these stars will precess because of the relativistic corrections to the black-hole's Newtonian field at rates

that depend directly on the compact object's spin and quadrupole moments (Will 2008).

The discovery of a single radio pulsar in orbit around Sgr A* will also allow for a direct measurement of the black hole's spin and quadrupole moment, by modeling relativistic effects in the residuals of its orbital solution (Wex & Kopeikin 1999). The presence of a cluster of young, massive stars in orbit around Sgr A* makes it highly likely that such pulsars exist (e.g., Pfahl & Loeb 2004) and current searches place a conservative upper limit of $\simeq 90$ pulsars within the central parsec of the galaxy (e.g., Macquart et al. 2010). The difficulty in detecting these pulsars lies in the fact that interstellar scattering heavily disperses and broadens the emission from each pulsar.

Finally, current mm-VLBI observations of Sgr A* with only three baselines have already confirmed the expectation that the accretion flow is optically thin at such wavelengths (Doeleman et al. 2008) and has led to the first constraints on the orientation and properties of the black hole (Broderick et al. 2009). Future observations with 5-10 baselines will provide the first direct image of horizon-scale structures in the vicinity of a black hole (Fish & Doeleman 2009) and allow for a model-independent measurement of the black-hole's spin and quadrupole moment (Johannsen & Psaltis 2010).

Measuring the mass, spin, and quadrupole moment of the black hole in the center of the Milky Way with three independent techniques is crucial in distinguishing relativistic effects from other astrophysical complications. Indeed, the presence of gas and stars in the vicinity of the black hole introduce perturbations to the orbits of stars and pulsars, that may mask or even bias the measurements. The cluster of stars (known and anticipated) in orbit around Sgr A* introduces multipole components to the gravitational field, which in turn cause preces-

sion of their orbits. In order for this classical effect to be negligible compared to the relativistic precession that depends on the spin and quadrupole of the black-hole spacetime, the orbital separations of the stars from the black hole have to be less than a milliparsec (Merritt et al. 2010).

Stars and pulsars orbiting very close to the black hole, however, will interact with the hot surrounding plasma, which is provided by the stellar winds of the more distant stars and powers the accretion luminosity of the black hole. This interaction will cause them to leave their geodesic orbits and very slowly spiral towards the black hole. If any of the various components of hydrodynamic drag is comparable to or larger than the perturbation to the Newtonian gravitational acceleration due to relativistic effects, then tracking the orbits of stars or pulsars around the black hole will not lead to a clean measurement of the moments of its spacetime.

In this article, I first infer the density and temperature of the hot plasma at different distances from Sgr A* using models of the accretion flow and of its feeding region that are consistent with current X-ray and millimeter observations. I then estimate the effect of hydrodynamic drag on the orbits of objects in this plasma and show that it is negligible for stars and pulsars orbiting within a few thousand gravitational radii from the black-hole horizon. Through this work, I will assume that the black hole has a mass of $4.5 \times 10^6 M_\odot$ and lies at a distance of 8.4 kpc, as inferred from the constrained fit of Ghez et al. (2008; see also Yelda et al. 2010).

2. THE DENSITY AND TEMPERATURE OF PLASMA AROUND SGR A*

The black hole in the center of the Milky Way is believed to be fed by the winds of massive stars that lie within the central parsec of the galaxy. A fraction of the mass lost by the stars is gravitationally captured and accreted by the black hole. Calculating the kinematics and thermodynamic properties of the plasma within the central plasma is non-trivial, as the flow is three-dimensional, with little symmetry, and variable at a large dynamic range of scales.

The feeding of the central black hole has been modeled in the past using multi-dimensional numerical simulations (e.g., Coker & Melia 1997; Rockefeller et al. 2004; Cuadra et al. 2006) or simpler, one-dimensional analytic models (e.g., Quataert 2004; Shcherbakov & Baganoff 2010). Both the analytic and numerical models use similar prescriptions for the mass-loss rates of the known stars and the newer works aim to reproduce the X-ray luminosity and temperature of the extended emission around Sgr A* as observed by the Chandra X-ray Observatory (Baganoff et al. 2003). For these reasons, the inferred density and temperature profiles of the plasma are very similar among the various models (see, e.g., Fig. 1 of Cuadra et al. 2006 for a comparison).

In this work, I will be using the semi-analytic model of Quataert (2004) as an estimate of the electron density and temperature of the plasma at distances $10^5 - 10^7 GM_{\text{BH}}/c^2$ from the black hole. Figure 1 shows these two properties of the plasma, both in the region probed by the Chandra observations (solid line) as well as extrapolated towards much smaller distances from the black hole (dashed line). The range of orbital separations

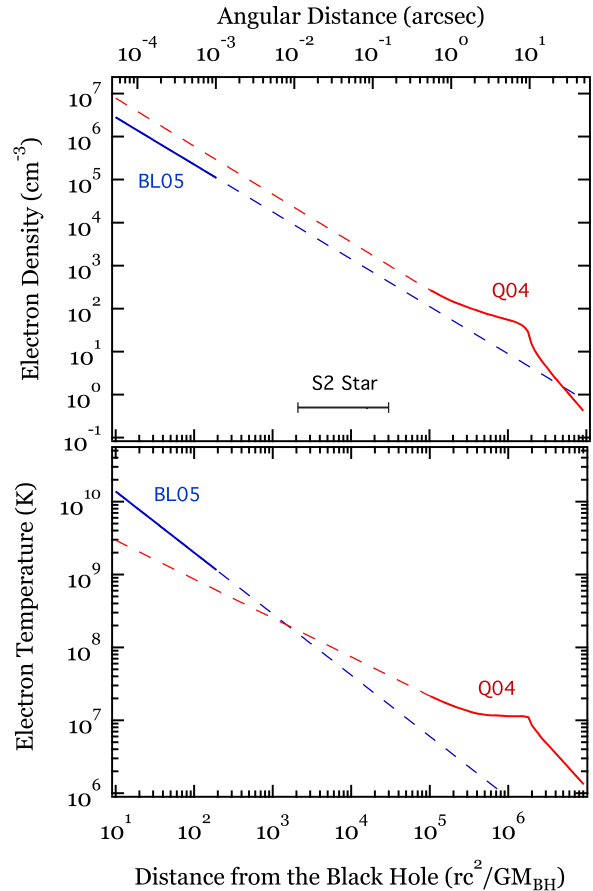


FIG. 1.— The inferred electron (*top*) density and (*bottom*) temperature at different distances from Sgr A*. At large distances, the model of Quataert (2004) was designed to fit the Chandra observations by Baganoff et al. (2003), who inferred the electron density and temperature of the extended emission around the black hole. At small distances, the model of Broderick & Loeb (2005) fits the long-wavelength spectrum of the accretion flow, is consistent with polarization measurements, and agrees with the size of the emitting region at 1.3 mm. The dashed portion of each curve represents an extrapolation of each model to distances far beyond its intended range of validity.

of the S2 star from the black hole, which is in the extrapolated regions of the curves, is also shown for comparison. The orbits of stars for which relativistic effects can be distinguished over gravitational perturbations from the stellar cluster itself will lie inside the orbit of the S2 star, shown with the horizontal solid line (Merritt et al. 2010). As a result, in order to estimate the effect of hydrodynamic drag on the orbits of nearby stars, I will need to investigate the validity of the extrapolation of the model towards small distances.

A second handle on the plasma properties near the black hole horizon is provided by the millimeter observations of Sgr A*, which probe the inner tens of gravitational radii of the accretion flow. During the last decade, analytic models of two-temperature, radiatively inefficient accretion flows have successfully accounted for the mm-to-cm spectra of Sgr A* (e.g., Narayan, Yi, & Mahadevan 1995), the polarization of its emission (Quataert & Gruzinov 2000; Agol 2000), as well as the size of its emitting region (Özel, Psaltis, & Narayan 2000).

Broderick & Loeb (2005; see also Broderick et al. 2009,

2011) constructed a semi-analytic model based on the earlier works and determined its parameters by fitting simultaneously the latest mm-to-cm spectra observed from Sgr A* (Falcke et al. 2008, Marrone et al. 2007), the polarization of its emission (Marrone et al. 2007), and the size of the emitting region at 1.3 mm (Doeleman et al. 2008). In their model, the electron density n_e and temperature T_e in the accretion flow scale with radius r as

$$n_e = n_e^0 \left(\frac{rc^2}{GM_{\text{BH}}} \right)^{-1.1} \quad (1)$$

and

$$T_e = T_e^0 \left(\frac{rc^2}{GM_{\text{BH}}} \right)^{-0.84}, \quad (2)$$

respectively, where M_{BH} is the mass of the black hole, G is the gravitational constant, and c is the speed of light. The best-fit parameters of the model to the observations are $n_e^0 = 3.5 \times 10^7 \text{ cm}^{-3}$ and $T_e^0 = 9.5 \times 10^{10} \text{ K}$ (Broderick et al. 2011). Independent MHD numerical simulations of radiatively inefficient accretion flows, which were compared to the same data, have reached similar conclusions regarding the overall scale of the electron density and temperature in the accretion flow (Mościbrodzka et al. 2009; Dexter et al. 2010).

Figure 1 compares the Broderick & Loeb (2005) model of the inner accretion flow to the Quataert (2004) model of the feeding region at large distances from the black hole. Remarkably, the inferred density of the inner accretion flow is only a factor of ~ 3 lower than the extrapolation of the Quataert (2004) model at distances that are smaller by four orders of magnitude compared to its intended region of validity (see also similar remarks in Shcherbakov & Baganoff 2010). In order to be conservative in calculating the effect of hydrodynamic drag on the orbits of objects around Sgr A*, I will use the extrapolation of the Quataert (2004) model throughout the vicinity of the black hole. Moreover, because in the regions of interest the electron temperature is in excess of 10^7 K (see below) I will assume that the plasma is fully ionized.

The electron temperature of the inner accretion flow is higher than the extrapolation of the Quataert (2004) model and has a steeper radial profile. This is not unexpected, however, as turbulent heating in the accretion flow will heat the plasma to temperatures higher than what is calculated in the analytical work, which takes into account only compressional and adiabatic heating. The discontinuity between the models is not a serious handicap for this calculation since I will use the plasma temperature only to infer whether the motion of objects through the plasma is sub-sonic or super-sonic. In order to achieve this, however, I will need to make an assumption regarding the ratio of ion-to-electron temperatures, as the models of both the inner accretion flow and of the feeding region provide an estimate of only the electron temperature in the plasma surrounding Sgr A*.

At large distances, ions and electrons are expected to have the same temperatures. On the other hand, close to the black hole, the combination of MHD simulations, which follow the dynamics of the ions, and of radiative transfer calculations, which model the electron properties, indicate that the ion temperature is $\sim 1 - 5$ times

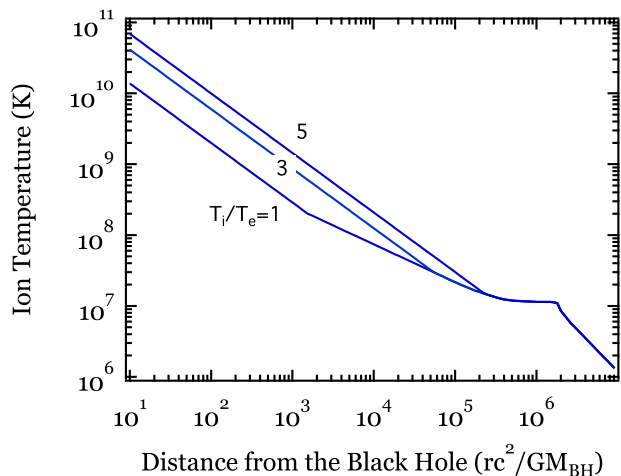


FIG. 2.— The inferred ion temperature of the accretion flow around Sgr A*. At large distances, it is set equal to the inferred electron temperature. At small distances, where the electrons are expected to be only weakly coupled with the ions, the ion temperature is believed to be $\sim 1 - 5$ times the electron temperature.

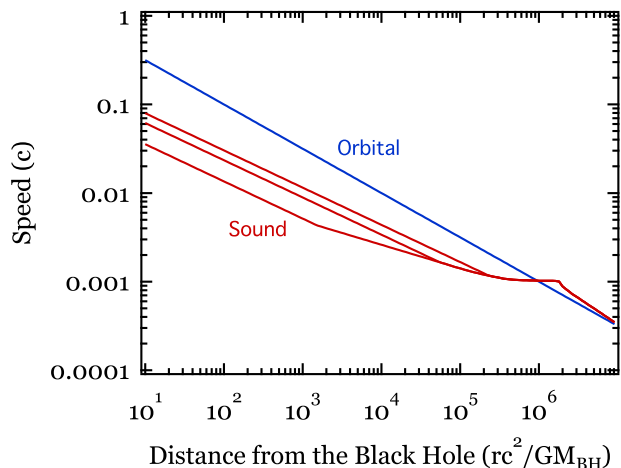


FIG. 3.— A comparison of the orbital speed to the local sound speed at different radii from Sgr A*. The sound speeds are calculated for the inferred electron temperatures shown in Figure 2. Throughout the inner region of the accretion flow, orbital speeds are mildly to highly supersonic.

the electron temperature (see, e.g., Mościbrodzka et al. 2009; Dexter et al. 2010). For the purposes of this work, I will use the temperature of the model by Quataert (2004) in the outer region of the plasma and an ion temperature that is $\simeq 1 - 5$ times the electron temperature of the Broderick & Loeb (2005) model in the inner region, where the latter is higher, as shown in Figure 2.

Figure 3 compares the sound speed in the models shown in Figure 2 to the characteristic orbital speed $u_{\text{orb}} = (GM_{\text{BH}}/r)^{1/2}$ at different distances from the black hole. In all regions of interest, i.e., for distances $\lesssim 10^5 M$, the orbital speed is larger than the local sound speed. As a result, the motion of stars and pulsars through the plasma surrounding Sgr A* will be mildly to highly supersonic.

3. THE INTERACTION OF STARS AND PULSARS WITH THE HOT PLASMA

The motion of a star or a pulsar in the vicinity of Sgr A* will be affected by its interaction with the surrounding plasma to the degree that it will preclude a clean gravitational experiment, if the interaction results in accelerations that are comparable to that of gravity. As a scale against which I will compare the hydrodynamic accelerations, the Newtonian gravitational acceleration at a distance r away from the central black hole is

$$a_N = \frac{GM_{\text{BH}}}{r^2} \simeq 1.4 \times 10^9 \left(\frac{M_{\text{BH}}}{4.5 \times 10^6 M_\odot} \right) \left(\frac{GM_{\text{BH}}}{rc^2} \right)^2 \text{ cm s}^{-2} \quad (3)$$

An observational verification of the no-hair theorem around Sgr A* will involve measuring the magnitude of the correction to the Newtonian acceleration that is proportional to the spin and the quadrupole moment of the black hole and verifying whether these lowest three multipole moments of its spacetime obey the relation of the Kerr metric. Corrections to the Newtonian acceleration that depend on the spin of the black hole are proportional to (see Merritt et al. 2010)

$$a_J = \frac{4\chi G^2 M_{\text{BH}}^2}{c^3} \left(\frac{u_{\text{orb}}}{r^3} \right) = 5.4 \times 10^9 \chi \left(\frac{M_{\text{BH}}}{4.5 \times 10^6 M_\odot} \right)^{-1} \left(\frac{GM_{\text{BH}}}{rc^2} \right)^{7/2} \text{ cm s}^{-2}, \quad (4)$$

where χ is the dimensionless spin of the black hole. Finally, corrections to the Newtonian acceleration that depend on the quadrupole moment of the spacetime, assuming that the latter is described by the Kerr solution, are proportional to (Merritt et al. 2010)

$$a_Q = \frac{3}{2} \chi^2 \left(\frac{G^3 M_{\text{BH}}^3}{c^2 r} \right)^4 = 2.0 \times 10^9 \chi^2 \left(\frac{M_{\text{BH}}}{4.5 \times 10^6 M_\odot} \right)^{-1} \left(\frac{GM_{\text{BH}}}{rc^2} \right)^4 \text{ cm s}^{-2}. \quad (5)$$

Figure 4 shows the magnitude of the various contributions to the gravitational acceleration at different distances from the central black hole, for an assumed spin of $\chi = 0.1$.

An orbiting object in the vicinity of Sgr A* interacts with the surrounding plasma in at least two distinct ways (see also Narayan 2000), which I will now consider in some detail.

First, as the object plows through the plasma, it scatters away the plasma particles or it gravitationally captures them, depending on its compactness. In the former case, the orbiting object transfers some of its linear momentum to the plasma particles, thereby feeling a hydrodynamic drag. In the latter case, the gravitational focusing of the trajectories of the plasma particles towards the back side of a small orbiting object leads to an increase of its linear momentum (Ruffer 1996). Which of the two cases dominates depends on the ratio of the Bondi radius to the radius of the object itself. Given

that the motion of stars and pulsars in the vicinity of Sgr A* is supersonic everywhere in the region of interest, I estimate the Bondi radius around such objects to be

$$R_B = \frac{2GM_*}{u_{\text{orb}}^2} = \frac{2GM_*}{c^2} \left(\frac{rc^2}{GM_{\text{BH}}} \right) \simeq 4 \times 10^{-5} \left(\frac{M_*}{10M_\odot} \right) \left(\frac{rc^2}{GM_{\text{BH}}} \right) R_\odot \simeq 6 \times 10^5 \left(\frac{M_*}{2M_\odot} \right) \left(\frac{rc^2}{GM_{\text{BH}}} \right) \text{ cm}. \quad (6)$$

In other words, the Bondi radius around a $10 M_\odot$ star is smaller than its stellar radius and, therefore, such a star will always feel a hydrodynamic drag. On the other hand, the Bondi radius around a neutron star is comparable to its size even at the smallest orbital separations from the central black hole and rapidly increases for larger orbits. As a result, Bondi accretion onto the neutron star will dominate the scattering of the plasma particles and lead to an increase of its orbital velocity.

I will estimate the magnitude of the acceleration due to the hydrodynamic drag a_d using the relation

$$M_* a_d \simeq \pi R_{\text{eff}}^2 \rho u_{\text{rel}}^2, \quad (7)$$

where ρ is the density of the plasma that I inferred in §2, u_{rel} is the relative velocity of the object with respect to the plasma, which I will set equal to the orbital velocity, and R_{eff} is the effective radius at which the moving object interacts with the plasma. For a normal star, the Bondi radius is much smaller than the stellar radius. I will, therefore, set the effective radius equal to the stellar radius R_* and obtain

$$a_d \simeq 1.1 \times 10^{-9} \left(\frac{M_*}{10M_\odot} \right)^{-1} \left(\frac{R_*}{10R_\odot} \right)^2 \left(\frac{n_e}{10^4 \text{ cm}^{-3}} \right) \left(\frac{GM_{\text{BH}}}{rc^2} \right) \text{ cm s}^{-2}, \quad (8)$$

where I have assumed a cosmic abundance of fully ionized material to express the mass density in terms of an electron density. Because the electron density in the accretion flow scales as $n_e \simeq r^{-1}$ (see §2), the acceleration due to the hydrodynamic drag scales as r^{-2} and, therefore, keeps an almost constant ratio with the Newtonian acceleration. Figure 4 compares the acceleration due to hydrodynamic drag to the various terms of the gravitational acceleration. Clearly, hydrodynamic drag on a $10 M_\odot$ star introduces only negligible perturbations to even the quadrupole term of the gravitational acceleration in all regions of interest. Note, however, that in the above estimates, I assumed a radius of the star that is typical for the main sequence. If the star is a giant, the acceleration due to the hydrodynamic drag will be significantly larger.

The hydrodynamic drag on a pulsar has a different dependence on the distance from the black hole compared to that of a $10 M_\odot$ star. The effective radius in this case is the Bondi radius, which increases linearly with increasing distance from the black hole. Setting $R_{\text{eff}} = R_B$ in equation (7), I obtain, for a $2 M_\odot$ neutron star,

$$a_d \simeq 6.2 \times 10^{-14} \left(\frac{M_*}{2M_\odot} \right)^{-1}$$

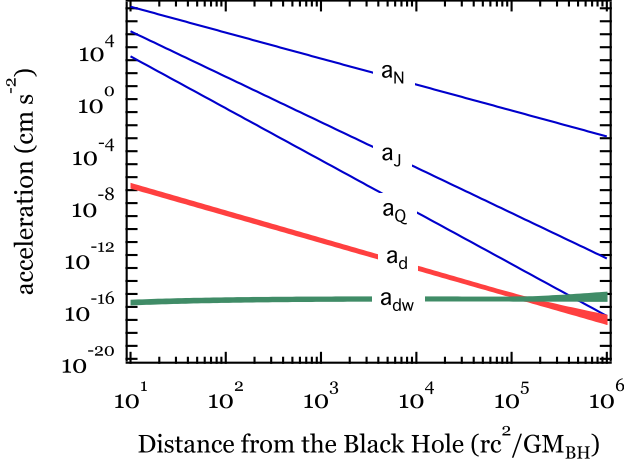


FIG. 4.— A comparison of various terms of the gravitational acceleration experienced by a star of mass $10 M_\odot$ and radius $10 R_\odot$ in orbit around Sgr A* (blue lines), to the acceleration due to hydrodynamic drag (a_d ; red line) and due to the gravitational interaction of the star with its wake (a_{dw} ; green line). The three blue lines correspond to the Newtonian acceleration (a_N), the term proportional to the spin of the black hole (a_J), and the term proportional to its quadrupole moment (a_Q). The black hole is assumed to be described by the Kerr solution and to be mildly spinning ($\chi = 0.1$). At radii $\lesssim 10^5 M$, hydrodynamic interactions are not large enough to preclude a successful measurement of the spin and quadrupole moment of the black hole.

$$\left(\frac{n_e}{10^4 \text{ cm}^{-3}}\right) \left(\frac{rc^2}{GM_{\text{BH}}}\right) \text{ cm s}^{-2}, \quad (9)$$

Figure 5 compares the hydrodynamic drag exerted on the neutron star to the various terms of the gravitational acceleration. Because the electron density in the region of interest scales as $n_e \sim r^{-1}$, the acceleration due to the hydrodynamic drag on the neutron star is nearly independent of the distance from the black hole. It becomes comparable to the quadrupole contribution to the gravitational acceleration at $\simeq 10^4$ gravitational radii.

As an object moves through the plasma in the vicinity of the black hole, it will also generate a wake behind it. The gravitational interaction between the object and the wake will result in an additional drag on the object, which will decelerate its motion. The magnitude of this effect has been calculated by Ostriker (1999) for the uniform motion of a star in a medium of constant density and more recently by Kim & Kim (2007, 2009) and Kim (2010) for the case of a circular motion in a stratified medium. The results of these papers were used by Narayan (2000) and by Barausse (2007) and Barausse & Rezzolla (2008) to estimate the effect of hydrodynamic drag on the properties of gravitational waves emitted during extreme mass-ratio inspirals.

Following these works, I estimate the magnitude of the resulting acceleration using the expression

$$M_* a_{dw} \simeq 4\pi \ln \left(\frac{R_{\text{max}}}{R_{\text{min}}} \right) \left(\frac{GM_*}{u_{\text{rel}}^2} \right) \rho. \quad (10)$$

Note that the drag due to the gravitational interaction with the wake decreases with increasing relative velocity, because as the velocity increases, the opening angle of the wake decreases.

For a $10 M_\odot$ star in orbit at radius r around the central black hole, the appropriate values for the maximum and

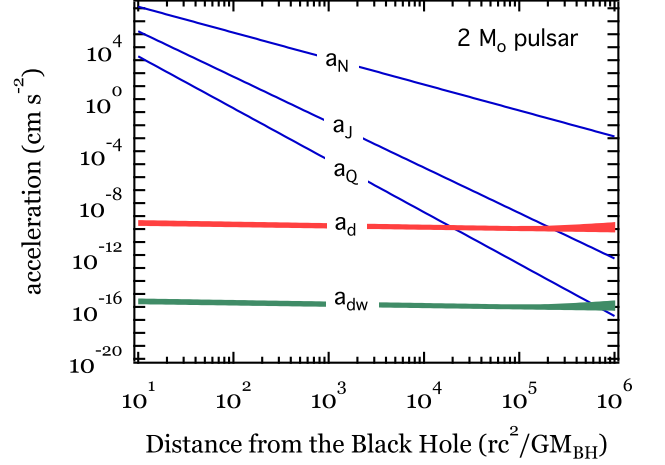


FIG. 5.— Same as in Figure 4 for a $2 M_\odot$ neutron star. At radii $\lesssim 10^4 M$, hydrodynamic interactions are not large enough to preclude a successful measurement of the spin and quadrupole moment of the black hole.

minimum distances of the wake are $R_{\text{max}} \simeq r$ and $R_{\text{min}} = R_*$, respectively. Setting, as above, the relative velocity equal to the orbital velocity u_{orb} , I obtain

$$a_{dw} = 9 \times 10^{-15} \left\{ \ln \left[\left(\frac{rc^2}{GM_{\text{BH}}} \right) \left(\frac{10 R_\odot}{R_*} \right) \right] - 0.046 \right\} \left(\frac{M_{\text{BH}}}{4.5 \times 10^6 M_\odot} \right) \left(\frac{n_e}{10^4 \text{ cm}^{-3}} \right) \left(\frac{rc^2}{GM_{\text{BH}}} \right) \text{ cm s}^{-2}.$$

Note that, because the electron density scales as $n_e \sim r^{-1}$, this acceleration is also nearly constant throughout the region of interest. Figure 4 compares the acceleration due to the interaction with the wake of a $10 M_\odot$ to the gravitational acceleration from the central black hole. Within $\simeq 10^6$ gravitational radii from the central black hole, this component of the hydrodynamic drag is negligible compared to the quadrupole component of the gravitational acceleration.

For the case of a $2 M_\odot$ neutron star, the minimum distance of the wake is the Bondi radius, i.e., $R_{\text{min}} = R_B$ and the acceleration due to the gravitational interaction of the star with its wake is

$$a_{dw} = 4.1 \times 10^{-21} \left\{ \ln \left[\left(\frac{M_{\text{BH}}}{4.5 \times 10^6 M_\odot} \right) \left(\frac{M_*}{2 M_\odot} \right)^{-1} \right] + 13.9 \right\} \left(\frac{M_*}{2 M_\odot} \right) \left(\frac{n_e}{10^4 \text{ cm}^{-3}} \right) \left(\frac{rc^2}{GM_{\text{BH}}} \right) \text{ cm s}^{-2}. \quad (11)$$

As before, the the acceleration due to the gravitational interaction of the neutron star with its wake depends only weakly on its distance from the black hole. Figure 5 compares the magnitude of this acceleration to the gravitational accelerations from the central black hole demonstrating that the former is again negligible in all regions of interest.

4. CONCLUSIONS

In this paper, I used the most recent models of the X-ray and millimeter observations of the black hole in the center of the Milky Way in order to estimate the density and temperature of the plasma in a wide range of distances from the central black hole. I then calculated the effect of hydrodynamic drag on the orbits of star and pulsars that can be used to probe relativistic effects and test the no-hair theorem.

I found that in both the case of orbiting stars and of pulsars, the hydrodynamic drag dominates over the gravitational interaction of the object with its wake. For the case of 10 M_{\odot} stars or 2 M_{\odot} pulsars around Sgr A*, the hydrodynamic drag is negligible compared to the quadrupole terms of the gravitational acceleration, as

long as their orbits are within $\simeq 10^5$ and $\simeq 10^4$ gravitational radii, respectively, from the central black hole. Albeit tight, such orbits are also required for the perturbations in the gravitational field due to the presence of the stellar cluster to be negligible compared to relativistic effects (Merritt et al. 2010). In other words, for those stars and pulsars for which the interactions with the other objects of the stellar cluster are negligible, hydrodynamic drag will not preclude measuring the spin and quadrupole moment of the black hole spacetime.

I thank Stefan Gillessen, Tim Johannsen, and Feryal Özel for useful comments on the manuscript. This work was supported by the NSF CAREER award NSF 0746549.

REFERENCES

- Agol, E. 2000, *ApJ*, 538, L121
 Baganoff, F. K., et al. 2003, *ApJ*, 591, 891
 Barausse, E. 2007, *MNRAS*, 382, 826
 Barausse, E., & Rezzolla, L. 2008, *Phys. Rev. D*, 77, 104027
 Broderick, A. E., & Loeb, A. 2005, *MNRAS*, 363, 353
 Broderick, A. E., Fish, V. L., Doeleman, S. S., & Loeb, A. 2009, *ApJ*, 697, 45
 ———. 2011, *ApJ*, 735, 110
 Chandrasekhar, S. 1943, *ApJ*, 97, 255
 Coker, R. F., & Melia, F. 1997, *ApJ*, 488, L149
 Cuadra, J., Nayakshin, S., Springel, V., & Di Matteo, T. 2006, *MNRAS*, 366, 358
 Dexter, J., Agol, E., Fragile, P. C., & McKinney, J. C. 2010, *ApJ*, 717, 1092
 Doeleman, S. S., et al. 2008, *Nature*, 455, 78
 Falcke, H., Goss, W. M., Matsuo, H., Teuben, P., Zhao, J.-H., & Zylka, R. 1998, *ApJ*, 499, 731
 Fish, V. L., & Doeleman, S. S. 2009, *arXiv:0906.4040*
 Ghez, A. M., et al. 2008, *ApJ*, 689, 1044
 Gillessen, S., Eisenhauer, F., Trippe, S., Alexander, T., Genzel, R., Martins, F., & Ott, T. 2009, *ApJ*, 692, 1075
 Gillessen, S., et al. 2010, *Proc. SPIE*, 7734,
 Johannsen, T., & Psaltis, D. 2010, *ApJ*, 718, 446
 Kim, H., & Kim, W.-T. 2007, *ApJ*, 665, 432
 ———. 2009, *ApJ*, 703, 1278
 Kim, W.-T. 2010, *ApJ*, 725, 1069
 Macquart, J.-P., Kanekar, N., Frail, D. A., & Ransom, S. M. 2010, *ApJ*, 715, 939
 Marrone, D. P., Moran, J. M., Zhao, J.-H., & Rao, R. 2007, *ApJ*, 654, L57
 Merritt, D., Alexander, T., Mikkola, S., & Will, C. M. 2010, *Phys. Rev. D*, 81, 062002
 Mościbrodzka, M., Gammie, C. F., Dolence, J. C., Shiokawa, H., & Leung, P. K. 2009, *ApJ*, 706, 497
 Narayan, R. 2000, *ApJ*, 536, 663
 Narayan, R., Yi, I., & Mahadevan, R. 1995, *Nature*, 374, 623
 Ostriker, E. C. 1999, *ApJ*, 513, 252
 Özel, F., Psaltis, D., & Narayan, R. 2000, *ApJ*, 541, 234
 Pfahl, E., & Loeb, A. 2004, *ApJ*, 615, 253
 Psaltis, D., & Johannsen, T. 2011, *Journal of Physics Conference Series*, 283, 012030
 Quataert, E. 2004, *ApJ*, 613, 322
 Quataert, E., & Gruzinov, A. 2000, *ApJ*, 545, 842
 Rockefeller, G., Fryer, C. L., Melia, F., & Warren, M. S. 2004, *ApJ*, 604, 662
 Ruffert, M. 1996, *A&A*, 311, 817
 Ryan, F. D. 1995, *Phys. Rev. D*, 52, 5707
 Sánchez-Salcedo, F. J., & Brandenburg, A. 1999, *ApJ*, 522, L35
 Shcherbakov, R. V., & Baganoff, F. K. 2010, *ApJ*, 716, 504
 Wex, N., & Kopeikin, S. M. 1999, *ApJ*, 514, 388
 Will, C. M. 2008, *ApJ*, 674, L25
 Yelda, S., Lu, J. R., Ghez, A. M., Clarkson, W., Anderson, J., Do, T., & Matthews, K. 2010, *ApJ*, 725, 331
 Yusef-Zadeh, F., et al. 2009, *ApJ*, 706, 348